Optimal Design of Voltage-Frequency Controllers for Microgrids

Mostafa Farrokhabadi, *Member, IEEE,* John W. Simpson-Porco, *Member, IEEE* and Claudio A. Cañizares, *Fellow, IEEE*

***Abstract*—This paper presents a systematic control synthesis framework for an optimal voltage-based frequency control (VFC) in islanded/isolated microgrids. A detailed model of a microgrid is first presented that is both scalable and generic. The problem of voltage-based frequency control is then formulated as an optimal $\mathcal{H}_\infty$ controller synthesis problem for the linearized microgrid model. The validity of model-reduction steps in which the feeders are neglected is discussed, and various centralized/decentralized control architectures are investigated. Multiple simulation studies are finally performed in MATLAB/Simulink to test and compare the performances of the control architectures in a microgrid test system. Simulation results confirm the robustness of the VFC controller with respect to simplifications in the system model, and realistic system changes compared to a non-optimal VFC.**

***Index Terms*—Microgrids, frequency control, stability, robust control.**

I. Introduction

A Microgrid is a cluster of loads and Distributed Energy Resources (DERs), including Renewable Energy Resources (RES) and Energy Storage Systems (ESS), that acts as a single controllable entity [1], [2]. Microgrids may operate in both grid-connected and islanded forms [3], and should be capable of seamless transition to islanded mode [4]. Isolated microgrids, e.g., those of remote communities, have no Point of Common Coupling with a larger grid.

Frequency control is a major challenge in isolated/islanded microgrids, in particular those with a higher penetration of electronically-interfaced DERs. First, in microgrid, mechanical rotational inertia is much lower compared to conventional networks, especially for high penetration of converter-based DERs, making them prone to large frequency deviations [5]. In addition, demand-supply balance is critical in microgrids, especially in isolated ones, due to the intermittent nature of RES [6], and the low number of generation units, which increases the risk of large disturbances due to generator outages [5]. Hence, an islanded/isolated microgrid experiences more frequent frequency deviations and a larger rate of change of frequency compared to a bulk power system. In this case, conventional frequency control techniques and tools, designed for large interconnected networks, may not be effective for microgrid frequency regulation, even in the presence of sufficient generation reserve [7].

M. Farrokhabadi is with BluWave-ai, Ottawa, ON, Canada (e-mail: m5farrok@uwaterloo.ca). J. W. Simpson-Porco and C. A. Cañizares are with the Department of Electrical and Computer Engineering, University of Waterloo, Waterloo, ON, N2L 3G1, Canada (e-mail: jwsimpson@uwaterloo.ca; ccanizares@uwaterloo.ca).

In view of the aforementioned frequency control challenges, numerous original and/or supplementary control techniques have been proposed in the literature [8], [9], including droop-based methods [10], [11], distributed cooperative controls [12], and central and/or hierarchical communication-based controls [13], [14]. All these control techniques are focused on proper power sharing among multiple DERs. Recently, the concept of a dynamic Voltage-based Frequency Controller (VFC) was introduced in [15] and [16], where it is shown that VFC acts as a virtual flywheel in the system, and compensates for the active power mismatch by changing the system operating voltages. Thus, the VFC operates in parallel to other power sharing techniques, and provides supplementary frequency control.

VFC is based on the strong coupling between voltage and frequency in microgrids, since due to the relatively short feeders of microgrids, voltage changes at the DERs terminals are almost instantaneously reflected on the load side, with limited voltage drops through the feeders, which in turn changes the system demand depending on the load voltage sensitivity indices [17], [18]. Thus, this tight voltage-frequency coupling is used to control frequency in the system by changing set-points of the voltage regulators (e.g., synchronous machine exciters).

A. Contributions

This paper presents a systematic disturbance rejecting control synthesis for voltage-based frequency control in islanded/isolated microgrids. The concept introduced in [15] is formalized and extended to evaluate various architectures for VFC, investigating the impact of each architecture on system small- and large- perturbation stability.

There are three major technical contributions. First, in Section II, a generic and scalable model of a microgrid is formulated and linearized, allowing to synthesize linear controllers and investigate microgrid stability. The added contribution compared to the previously proposed models (e.g., [19], [20]) is that the modeling approach presented here is highly scalable and optimized for computer implementation; incidence matrices are introduced and integrated in the formulation process, allowing for easy re-structuring and/or addition/removal of microgrid components. Discussion is provided on proper per-unitization of system components and parameters.

Second, in Section III-B, a detailed discussion on the impact of feeders in microgrid studies is given, in particular for VFC synthesis. It has been previously argued that network in microgrids may not play a significant role in the performance of control and optimization techniques [21], in particular because feeders are short and their static capacity is much greater than the maximum system demand [22], [23]. Conditions under which network simplifications and/or elimination would be a reasonable are identified and discussed.

Third and finally, a systematic framework is presented for VFC design through LMI-based minimization of the $\mathcal{H}_\infty$ gain from active power disturbances to frequency deviations in the microgrid in Section III. The presented control synthesis has considerable advantages over the trail-and-error-based tuning of a fixed structure controller presented in [15], where the presented controller is limited to systems with one voltage regulator or multiple identical voltage regulators, whereas the systematic control synthesis presented in this paper allows for one-step design of VFC for all (potentially heterogeneous) voltage regulators. In Section IV, various structures of VFC are designed, including both SISO and MIMO controllers, and their closed-loop performance and robustness are compared via extensive simulations on a modified CIGRE test system to identify the most effective, practical, and computationally efficient control framework.

B. Notation

Let $\mathbb{R}$ denote the set of real numbers, Id_n denote the $n \times n$ identity matrix. A matrix of zeros of appropriate dimensions is $\mathbb{0}$, while $\mathbb{1}_n$ denotes a column n-vector of all ones. The symbol $\otimes$ denotes the Kronecker product; for later let $\mathbf{j} = \sqrt{-1}$, $J := \left[\begin{smallmatrix} 0 & 1 \\ -1 & 0 \end{smallmatrix}\right]$, and $\mathcal{J}_n := \mathrm{Id}_n \otimes J$. Given matrices A and B, $\mathrm{blkdiag}(A, B) = \left[\begin{smallmatrix} A & \mathbb{0} \\ \mathbb{0} & B \end{smallmatrix}\right]$. For a set of scalars or vectors $v_1, \ldots, v_n$, $\mathrm{col}(v_1, \ldots, v_n)$ denotes the stacked column matrix of all entries. The notation $A \in \{0,1\}^{n \times m}$ means $A \in \mathbb{R}^{n \times m}$ with all elements being either zero or one.

II. General Microgrid Model

This section presents a general and modular model of a microgrid consisting of Π-model feeders, synchronous machines, power converters, and exponential static load models.

A. Network Model

A balanced three-phase AC microgrid with base frequency ω_{bse} and base voltage V_{bse} is considered here; all quantities in this paper are in per-unit values except for time. The microgrid has n_{b} buses with index set $\mathcal{N}_{\mathrm{b}} = \{1, \ldots, n_{\mathrm{b}}\}$, n_{sg} synchronous generators with index set $\mathcal{N}_{\mathrm{sg}} = \{1, \ldots, n_{\mathrm{sg}}\}$, n_{ld} loads with index set $\mathcal{N}_{\mathrm{ld}}$, and n_{pc} power converters with index set $\mathcal{N}_{\mathrm{pc}}$. The topology of the network (and associated reference directions for current flows and voltage drops) is described by a connected oriented graph $(\mathcal{N}_{\mathrm{b}}, \mathcal{E})$, with $\mathcal{E} \subset \mathcal{N}_{\mathrm{b}} \times \mathcal{N}_{\mathrm{b}}$ denoting the set of n_{br} (three-phase) branches of the form (j, k) with $j, k \in \mathcal{N}_{\mathrm{b}}$. An arbitrary ordering to these n_{br} branches is used and uniquely labeled as $\mathcal{N}_{\mathrm{br}} = \{1, \ldots, n_{\mathrm{br}}\}$. The microgrid topology may then be encoded in the *bus-branch incidence matrix* $A \in \mathbb{R}^{n_{\mathrm{b}} \times n_{\mathrm{br}}}$, defined component-wise as $A_{je} = +1$ if branch $e \sim (j, k)$ for some bus k, $A_{je} = -1$ if $e \sim (k, j)$ for some bus k, and zero otherwise. For later use, $\mathcal{A}_m := A \otimes \mathrm{Id}_m \in \mathbb{R}^{m \cdot n_{\mathrm{b}} \times m \cdot n_{\mathrm{br}}}$, with $\mathcal{A}_2$ denoted more simply as $\mathcal{A}$.

Associated with each bus $k \in \mathcal{N}_{\mathrm{b}}$ is a three-phase bus-to-ground potential $V_k \in \mathbb{R}^3$ and a three-phase current injection $I_k \in \mathbb{R}^3$, while each branch $(j, k) \in \mathcal{E}$ has a three-phase oriented current flow $i_{jk} \in \mathbb{R}^3$ and a three-phase oriented voltage drop $v_{jk} \in \mathbb{R}^3$. These variables are related to one another via KCL and KVL, expressed through the incidence matrix as follows [24]:

$$\begin{bmatrix} I_1 \\ \vdots \\ I_{n_{\mathrm{b}}} \end{bmatrix} = \mathcal{A}_3 \begin{bmatrix} i_1 \\ \vdots \\ i_{n_{\mathrm{br}}} \end{bmatrix}, \quad \begin{bmatrix} v_1 \\ \vdots \\ v_{n_{\mathrm{br}}} \end{bmatrix} = \mathcal{A}_3^{\mathsf{T}} \begin{bmatrix} V_1 \\ \vdots \\ V_{n_{\mathrm{b}}} \end{bmatrix} \tag{1}$$

For each branch $(j, k) \in \mathcal{E}$ (and for each bus $k \in \mathcal{N}_{\mathrm{b}}$), and has a three-phase KVL (or KCL) equation:

$$\begin{aligned} \frac{1}{\omega_{\mathrm{bse}}} L_{jk} \frac{\mathrm{d}i_{jk}}{\mathrm{d}t} &= -R_{jk} i_{jk} + v_{jk}\,, \qquad (j,k) \in \mathcal{E}\,, \\ \frac{1}{\omega_{\mathrm{bse}}} C_k \frac{\mathrm{d}V_k}{\mathrm{d}t} &= -G_k V_k + I_k\,, \qquad k \in \mathcal{N}_{\mathrm{b}}\,, \end{aligned} \tag{2}$$

where $R_{jk}, L_{jk} > 0$ are the resistances and inductances for line (j, k); note that these parameters are the same for all phases of branch (j, k).

To convert this three-phase equation to a rotating dq reference frame, let $\theta_{\mathrm{G}} \in \mathbb{R}$ be a global reference angle, let $T : \mathbb{R} \to \mathbb{R}^{2 \times 3}$ be the abc to dq transformation matrix:

$$T(\theta_{\mathrm{G}}) = \frac{2}{3} \begin{bmatrix} \sin(\theta_{\mathrm{G}}) & \sin(\theta_{\mathrm{G}} - 2\pi/3) & \sin(\theta_{\mathrm{G}} + 2\pi/3) \\ \cos(\theta_{\mathrm{G}}) & \cos(\theta_{\mathrm{G}} - 2\pi/3) & \cos(\theta_{\mathrm{G}} + 2\pi/3) \end{bmatrix}$$

and let:

$$\begin{aligned} V_{\mathrm{DQ},k} &= \mathrm{col}(V_{\mathrm{D},k}, V_{\mathrm{Q},k}) &&:= T(\theta_{\mathrm{G}}) V_k \\ v_{\mathrm{DQ},jk} &= \mathrm{col}(v_{\mathrm{D},jk}, v_{\mathrm{Q},jk}) &&:= T(\theta_{\mathrm{G}}) v_{jk} \\ I_{\mathrm{DQ},k} &= \mathrm{col}(I_{\mathrm{D},k}, I_{\mathrm{Q},k}) &&:= T(\theta_{\mathrm{G}}) I_k \\ i_{\mathrm{DQ},jk} &= \mathrm{col}(i_{\mathrm{D},jk}, i_{\mathrm{Q},jk}) &&:= T(\theta_{\mathrm{G}}) i_{jk}\,, \end{aligned}$$

be the transformed potential, voltage, and current variables. Then in the new coordinates, the $3n_{\mathrm{br}} + 3n_{\mathrm{b}}$ equations (2) are transformed to the following $2n_{\mathrm{br}} + 2n_{\mathrm{b}}$ equations:

$$\begin{aligned} \frac{L_{jk}}{\omega_{\mathrm{bse}}} \frac{\mathrm{d}}{\mathrm{d}t} \begin{bmatrix} i_{\mathrm{D},jk} \\ i_{\mathrm{Q},jk} \end{bmatrix} &= \begin{bmatrix} -R_{jk} i_{\mathrm{D},jk} + \omega_{\mathrm{G}} L_{jk} i_{\mathrm{Q},jk} \\ -\omega_{\mathrm{G}} L_{jk} i_{\mathrm{D},jk} - R_{jk} i_{\mathrm{Q},jk} \end{bmatrix} + \begin{bmatrix} v_{\mathrm{D},jk} \\ v_{\mathrm{Q},jk} \end{bmatrix} \\ \frac{C_k}{\omega_{\mathrm{bse}}} \frac{\mathrm{d}}{\mathrm{d}t} \begin{bmatrix} V_{\mathrm{D},k} \\ V_{\mathrm{Q},k} \end{bmatrix} &= \begin{bmatrix} -G_k V_{\mathrm{D},k} + \omega_{\mathrm{G}} C_k V_{\mathrm{Q},k} \\ -\omega_{\mathrm{G}} C_k V_{\mathrm{D},k} - G_k V_{\mathrm{Q},k} \end{bmatrix} + \begin{bmatrix} I_{\mathrm{D},k} \\ I_{\mathrm{Q},k} \end{bmatrix} \end{aligned} \tag{3}$$

where $\omega_{\mathrm{G}} = \dot{\theta}_{\mathrm{G}}$. Write (3) in vector notation, let

$$i_{\mathrm{DQ}} := \mathrm{col}(i_{\mathrm{DQ},1}\,, i_{\mathrm{DQ},2}\,, \ldots\,, i_{\mathrm{DQ},n_{\mathrm{br}}}) \in \mathbb{R}^{2n_{\mathrm{br}}}$$

be the stacked vector of all current flow variables, with $V_{\mathrm{DQ}}, v_{\mathrm{DQ}}$, and I_{DQ} defined analogously. The KCL/KVL equations (1) now reads in dq coordinates as follows:

$$I_{\mathrm{DQ}} = \mathcal{A} i_{\mathrm{DQ}} + I_{\mathrm{DQ}}^{\mathrm{ext}}\,, \qquad v_{\mathrm{DQ}} = \mathcal{A}^{\mathsf{T}} V_{\mathrm{DQ}}\,, \tag{4}$$

where $I_{\mathrm{DQ}}^{\mathrm{ext}} \in \mathbb{R}^{2n_{\mathrm{b}}}$ is introduced as the vector of additional external current injections, through which loads, generators, and converters will be interfaced as follows:

$$I_{\mathrm{DQ}}^{\mathrm{ext}} = I_{\mathrm{DQ}}^{\mathrm{ld}} + I_{\mathrm{DQ}}^{\mathrm{sg}} + I_{\mathrm{DQ}}^{\mathrm{conv}}\,.$$

To shorten the formulas, let $L_{\mathrm{br}} := \mathrm{blkdiag}\left(L_{jk} \mathrm{Id}_2\right)_{(j,k) \in \mathcal{E}}$ be the diagonal matrix of branch inductances, with $R_{\mathrm{br}}, G_{\mathrm{b}}$, and C_{b} defined analogously. Then the network dynamics (3) becomes the following vectorized state-space model:

$$\begin{aligned}\frac{1}{\omega_{\mathrm{bse}}}\frac{\mathrm{d}}{\mathrm{d}t}\begin{bmatrix}L_{\mathrm{br}} & \mathbb{0}\\ \mathbb{0} & C_{\mathrm{b}}\end{bmatrix}\begin{bmatrix}i_{\mathrm{DQ}}\\ V_{\mathrm{DQ}}\end{bmatrix} &= \begin{bmatrix}\mathbb{0}\\ I_{\mathrm{DQ}}^{\mathrm{ext}}\end{bmatrix}\\ &+\begin{bmatrix}-R_{\mathrm{br}}+\omega_{\mathrm{G}}L_{\mathrm{br}}\mathcal{J}_{\mathrm{br}} & \mathcal{A}^{\mathsf{T}}\\ \mathcal{A} & -G_{\mathrm{b}}+\omega_{\mathrm{G}}C_{\mathrm{b}}\mathcal{J}_{\mathrm{b}}\end{bmatrix}\begin{bmatrix}i_{\mathrm{DQ}}\\ V_{\mathrm{DQ}}\end{bmatrix},\end{aligned} \tag{5}$$

where $\mathcal{J}_{\mathrm{br}} := \mathrm{Id}_{n_{\mathrm{br}}} \otimes J$ and $\mathcal{J}_{\mathrm{b}} := \mathrm{Id}_{n_{\mathrm{b}}} \otimes J$. The network model has internal states $x^{\mathrm{net}} := \mathrm{col}(i_{\mathrm{DQ}}, V_{\mathrm{DQ}})$, inputs $u^{\mathrm{net}} = \mathrm{col}(\omega_{\mathrm{G}}, I_{\mathrm{DQ}}^{\mathrm{ext}})$, and outputs $y_{\mathrm{net}} = V_{\mathrm{DQ}}$. Around an equilibrium state-input pair $\{(x^{\mathrm{net}})^\star, (u^{\mathrm{net}})^\star\}$, (5) can be linearized and put into state-space form as follows:

$$\begin{aligned}\Delta\dot{x}^{\mathrm{net}} &= A^{\mathrm{net}}\Delta x^{\mathrm{net}} + B_{\mathrm{G}}^{\mathrm{net}}\Delta\omega_G + B_{\mathrm{DQ}}^{\mathrm{net}}\Delta I_{\mathrm{DQ}}^{\mathrm{ext}}\\ \Delta V_{\mathrm{DQ}} &= C_{\mathrm{DQ}}^{\mathrm{net}}\Delta x^{\mathrm{net}}\end{aligned} \tag{6}$$

where $\Delta z = z - z^\star$ is the deviation of z around $z^\star$ and:

$$\begin{aligned}A^{\mathrm{net}} &= M_{\mathrm{net}}^{-1}\begin{bmatrix}-R_{\mathrm{br}}+\omega_{\mathrm{G}}^\star L_{\mathrm{br}}\mathcal{J}_{\mathrm{br}} & \mathcal{A}^{\mathsf{T}}\\ \mathcal{A} & -G_{\mathrm{b}}+\omega_{\mathrm{G}}^\star C_{\mathrm{b}}\mathcal{J}_{\mathrm{b}}\end{bmatrix}\\ B_G^{\mathrm{net}} &= M_{\mathrm{net}}^{-1}\begin{bmatrix}L_{\mathrm{br}}\mathcal{J}_{\mathrm{br}}i_{\mathrm{DQ}}^\star\\ C_{\mathrm{b}}\mathcal{J}_{\mathrm{b}}V_{\mathrm{DQ}}^\star\end{bmatrix},\ B_{\mathrm{DQ}}^{\mathrm{net}} = M_{\mathrm{net}}^{-1}\begin{bmatrix}\mathbb{0}\\ \mathrm{Id}_{2n_{\mathrm{b}}}\end{bmatrix}\\ C_{\mathrm{DQ}}^{\mathrm{net}} &= \begin{bmatrix}\mathbb{0} & \mathrm{Id}_{2n_{\mathrm{b}}}\end{bmatrix}, \quad M_{\mathrm{net}} = \frac{1}{\omega_{\mathrm{bse}}}\mathrm{blkdiag}(L_{\mathrm{br}}, C_{\mathrm{b}}).\end{aligned} \tag{7}$$

B. Voltage-Sensitive Load Models

For each load $k \in \mathcal{N}_{\mathrm{ld}}$, exponential load models are considered, in which the (per-unit) instantaneous active and reactive power injections P_k^{ld} and Q_k^{ld} at bus $k \in \mathcal{N}_{\mathrm{ld}}$ are proportional to the (per unit) bus voltage magnitude raised to some power as follows:

$$\begin{aligned}P_k^{\mathrm{ld}} &= \mathcal{P}_k(V_k)^{m_k}, \quad Q_k^{\mathrm{ld}} = \mathcal{Q}_k(V_k)^{n_k},\\ V_k^2 &= V_{\mathrm{D},k}^2 + V_{\mathrm{Q},k}^2 = V_{\mathrm{DQ},k}^{\mathsf{T}}V_{\mathrm{DQ},k}.\end{aligned} \tag{8}$$

Here, $n_k, m_k \geq 0$ are coefficients describing the load model, and $\mathcal{P}_k$ and $\mathcal{Q}_k$ are the per-unit instantaneous active/reactive power consumptions at base voltage. To introduce load disturbances, the parameters $\mathcal{P}_k$ and $\mathcal{Q}_k$ will have nominal values $\mathcal{P}_k^\star$ and $\mathcal{Q}_k^\star$, which can be subject to changes $\Delta\mathcal{P}_k$ and $\Delta\mathcal{Q}_k$, respectively. The instantaneous active and reactive power for the load are determined in terms of the load current and bus voltage as follows:

$$\begin{aligned}P_k^{\mathrm{ld}} &= I_{\mathrm{D},k}^{\mathrm{ld}}V_{\mathrm{D},k} + I_{\mathrm{Q},k}^{\mathrm{ld}}V_{\mathrm{Q},k} = (I_{\mathrm{DQ},k}^{\mathrm{ld}})^{\mathsf{T}}V_{\mathrm{DQ},k}\\ Q_k^{\mathrm{ld}} &= I_{\mathrm{D},k}^{\mathrm{ld}}V_{\mathrm{Q},k} - I_{\mathrm{Q},k}^{\mathrm{ld}}V_{\mathrm{D},k} = (I_{\mathrm{DQ},k}^{\mathrm{ld}})^{\mathsf{T}}\,J\,V_{\mathrm{DQ},k}.\end{aligned} \tag{9}$$

Combining the previous equations, for each $k \in \mathcal{N}_{\mathrm{ld}}$ yields:

$$\begin{aligned}0 &= \mathcal{P}_k\left(V_{\mathrm{DQ},k}^{\mathsf{T}}V_{\mathrm{DQ},k}\right)^{\frac{m_k}{2}} - (I_{\mathrm{DQ},k}^{\mathrm{ld}})^{\mathsf{T}}V_{\mathrm{DQ},k}\\ 0 &= \mathcal{Q}_k\left(V_{\mathrm{DQ},k}^{\mathsf{T}}V_{\mathrm{DQ},k}\right)^{\frac{n_k}{2}} - (I_{\mathrm{DQ},k}^{\mathrm{ld}})^{\mathsf{T}}\,J\,V_{\mathrm{DQ},k}.\end{aligned} \tag{10}$$

Around an operating point $\{(V_{\mathrm{DQ}}^{\mathrm{ld}})^\star, (I_{\mathrm{DQ}}^{\mathrm{ld}})^\star, \mathcal{P}^\star, \mathcal{Q}^\star\}$, the $2n_{\mathrm{ld}}$ load equations (10) may be linearized and rearranged to obtain a vectorized expression of the form

$$\Delta I_{\mathrm{DQ}}^{\mathrm{ld}} = A^{\mathrm{ld}}\Delta V_{\mathrm{DQ}}^{\mathrm{ld}} + E^{\mathrm{ld}}\Delta S^{\mathrm{ld}} \tag{11}$$

where $\Delta S^{\mathrm{ld}} = \mathrm{col}(\Delta\mathcal{P}_1, \Delta\mathcal{Q}_1, \ldots, \Delta\mathcal{P}_{n_{\mathrm{ld}}}, \Delta\mathcal{Q}_{n_{\mathrm{ld}}})$ is the vector of power disturbances. The matrices $A^{\mathrm{ld}}, E^{\mathrm{ld}} \in \mathbb{R}^{2n_{\mathrm{ld}}\times 2n_{\mathrm{ld}}}$ are block diagonal with n_{ld} 2x2 blocks, given by

$$\begin{aligned}A_k^{\mathrm{ld}} &= \begin{bmatrix}V_{\mathrm{DQ},k}^{\mathsf{T}}\\ V_{\mathrm{DQ},k}^{\mathsf{T}}J^{\mathsf{T}}\end{bmatrix}^{-1}\begin{bmatrix}\mathcal{P}_k\gamma(V_{\mathrm{DQ},k}, m_k) - (I_{\mathrm{DQ},k}^{\mathrm{ld}})^{\mathsf{T}}\\ \mathcal{Q}_k\gamma(V_{\mathrm{DQ},k}, n_k) - (I_{\mathrm{DQ},k}^{\mathrm{ld}})^{\mathsf{T}}\end{bmatrix}\Bigg|_{\text{op. pt.}}\\ E_k^{\mathrm{ld}} &= \begin{bmatrix}V_{\mathrm{DQ},k}^{\mathsf{T}}\\ V_{\mathrm{DQ},k}^{\mathsf{T}}J^{\mathsf{T}}\end{bmatrix}^{-1}\begin{bmatrix}\kappa(V_{\mathrm{DQ},k}, m_k) & 0\\ 0 & \kappa(V_{\mathrm{DQ},k}, m_k)\end{bmatrix}\Bigg|_{\text{op. pt.}}\end{aligned}$$

where $\gamma(z,\beta) = \beta(z^{\mathsf{T}}z)^{\frac{\beta}{2}-1}z^{\mathsf{T}}$ and $\kappa(z,\beta) = (z^{\mathsf{T}}z)^{\frac{\beta}{2}}$.

C. Synchronous Generators

The dynamic model of the kth synchronous machine has a mechanical subsystem, where states are the rotor angle δ_k and angular frequency ω_k, equipped with a Woodward governor model with associated state vector $x_{\mathrm{gov},k} \in \mathbb{R}^5$; the governor reference frequency $\omega_{\mathrm{ref},k}$ is assumed to be constant. The machine has an electrical subsystem ($i_{\mathrm{gen},k} \in \mathbb{R}^6$) equipped with a one state exciter model ($e_{\mathrm{fd},k} \in \mathbb{R}$). All models are written in the the local rotor reference frame of the machine.

The voltage set-point $V_{\mathrm{ref},k}$ for the exciter is separated into a nominal set-point $V_{\mathrm{ref},k}^\star$ and a modulation term $\Delta v_{\mathrm{ref},k}$, as $V_{\mathrm{ref},k} = V_{\mathrm{ref},k}^\star + \Delta v_{\mathrm{ref},k}$. The external inputs to the model are the exciter voltage reference modulation $\Delta v_{\mathrm{ref},k}$, and the local dq frame terminal voltage vector $v_{\mathrm{dq},k} = \mathrm{col}(v_{\mathrm{d},k}, v_{\mathrm{q},k})$; the latter are the inputs through which the generator is interfaced with the network. The output of the generator model is the local dq frame current injection $i_{\mathrm{dq},k} = \mathrm{col}(i_{\mathrm{d},k}, i_{\mathrm{q},k})$. The overall nonlinear state-state model of generator $k \in \mathcal{N}_{\mathrm{sg}}$ is of the following form:

$$\begin{aligned}\dot{x}_k^{\mathrm{gen}} &= \tilde{f}_k^{\mathrm{sg}}(x_k^{\mathrm{sg}}, v_{\mathrm{dq},k}) + B_{v,k}^{\mathrm{sg}}\Delta v_{\mathrm{ref},k}\\ i_{\mathrm{dq},k} &= c_k^{\mathrm{sg}}x_k^{\mathrm{gen}}\end{aligned} \tag{12}$$

with state vector

$$x_k^{\mathrm{sg}} = (\delta_k, \omega_k, x_{\mathrm{gov},k}, i_{\mathrm{gen},k}, e_{\mathrm{fd},k})^{\mathsf{T}} \in \mathbb{R}^{14},$$

where $\tilde{f}_k^{\mathrm{sg}} : \mathbb{R}^{14}\times\mathbb{R}^2 \to \mathbb{R}^{14}$ describes the generator dynamics and $B_{v,k}^{\mathrm{sg}} \in \mathbb{R}^{14\times 1}, c_k^{\mathrm{sg}} \in \mathbb{R}^{2\times 14}$ are appropriate matrices.

The generator equations are expressed in the local rotor dq reference frame rotating at speed ω_k. To interface each generator model with the network model, the coupling input and output variables are transformed to the global dq reference frame rotating at speed ω_{G} via the local-to-global transformation matrix $\mathcal{T} : \mathbb{R}\times\mathbb{R} \to \mathbb{R}^{2\times 2}$ defined by [25]:

$$\mathcal{T}(\theta_{\mathrm{G}}, \delta_k) := \begin{bmatrix}\cos(\theta_{\mathrm{G}}-\delta_k) & \sin(\theta_{\mathrm{G}}-\delta_k)\\ -\sin(\theta_{\mathrm{G}}-\delta_k) & \cos(\theta_{\mathrm{G}}-\delta_k)\end{bmatrix}, \tag{13}$$

which satisfies $\mathcal{T}(\theta_{\mathrm{G}}, \delta_k)^{-1} = \mathcal{T}(\theta_{\mathrm{G}}, \delta_k)^{\mathsf{T}}$. Hence,

$$I_{\mathrm{DQ},k}^{\mathrm{sg}} = \mathcal{T}(\theta_{\mathrm{G}}, \delta_k)i_{\mathrm{dq},k}, \quad V_{\mathrm{DQ},k}^{\mathrm{sg}} = \mathcal{T}(\theta_{\mathrm{G}}, \delta_k)v_{\mathrm{dq},k}.$$

With this transformation of inputs and outputs, the state-space model is:

$$\begin{aligned}\dot{x}_k^{\mathrm{sg}} &= f_k^{\mathrm{sg}}(x_k^{\mathrm{sg}}, \theta_{\mathrm{G}}, V_{\mathrm{DQ},k}^{\mathrm{sg}}) + B_{v,k}^{\mathrm{sg}}\Delta v_{\mathrm{ref},k}\\ I_{\mathrm{DQ},k}^{\mathrm{sg}} &= \mathcal{T}(\theta_{\mathrm{G}}, \delta_k)c_k^{\mathrm{sg}}x_k^{\mathrm{sg}},\end{aligned}$$

with network inputs $V^{\rm sg}_{{\rm DQ},k} \in \mathbb{R}^2$ and outputs $I^{\rm sg}_{{\rm DQ},k} \in \mathbb{R}^2$, and where $f^{\rm sg}_k(x^{\rm sg}_k, \theta_{\rm G}, V^{\rm sg}_{{\rm DQ},k}) := \tilde{f}^{\rm sg}_k(x^{\rm sg}_k, \mathcal{T}(\theta_{\rm G}, \delta_k)^{\mathsf T} V^{\rm sg}_{{\rm DQ},k})$. Putting these equations all together for all generators $k \in \mathcal{N}_{\rm sg}$, the stacked nonlinear input-output system are:

$$\begin{aligned} \dot{x}^{\rm sg} &= f^{\rm sg}(x^{\rm sg}, \theta_{\rm G}, V^{\rm sg}_{\rm DQ}) + B^{\rm sg}_v \Delta v_{\rm ref} \\ I^{\rm sg}_{\rm DQ} &= h^{\rm sg}(x^{\rm sg}, \theta_{\rm G}) \,. \end{aligned} \tag{14}$$

For the global reference angle, the first generator rotor angle is arbitrarily selected * and set to $\theta_{\rm G} = \delta_1$, $\omega_{\rm G} = \omega_1$. It follows that around an operating point $(x^\star_{\rm sg}, (V^{\rm sg}_{\rm DQ})^\star, (I^{\rm sg}_{\rm DQ})^\star, \Delta v^\star_{\rm ref} = \mathbb{0})$, the dynamics (14) can be linearized to obtain the model:

$$\begin{aligned} \Delta\dot{x}^{\rm sg} &= A^{\rm sg}\Delta x^{\rm sg} + B^{\rm sg}_{\rm DQ}\Delta V^{\rm sg}_{\rm DQ} + B^{\rm sg}_v \Delta v_{\rm ref} \\ \Delta I^{\rm sg}_{\rm DQ} &= C^{\rm sg}_{\rm DQ}\Delta x^{\rm sg} \,, \\ \Delta\omega^{\rm sg} &= C^{\rm sg}_{\omega}\Delta x^{\rm sg} \\ \Delta\theta_G &= C^{\rm sg}_{\theta_G}\Delta x^{\rm sg} = \left[\begin{array}{c|c} 1 & \mathbb{0}^{\mathsf T}_{14n_{\rm sg}-1} \end{array}\right] \Delta x^{\rm sg} \\ \Delta\omega_G &= C^{\rm sg}_{\omega_G}\Delta x^{\rm sg} = \left[\begin{array}{cc|c} 0 & 1 & \mathbb{0}^{\mathsf T}_{14n_{\rm sg}-2} \end{array}\right] \Delta x^{\rm sg} \end{aligned} \tag{15}$$

where $A^{\rm sg} \in \mathbb{R}^{14n_{\rm sg}\times 14n_{\rm sg}}$, $B^{\rm sg}_{\rm DQ} \in \mathbb{R}^{14n_{\rm sg}\times 2n_{\rm sg}}$, $B^{\rm sg}_v \in \mathbb{R}^{14n_{\rm sg}\times n_{\rm sg}}$ and $C^{\rm sg}_{\rm DQ} \in \mathbb{R}^{2n_{\rm sg}\times 14n_{\rm sg}}$ are appropriate matrices. The additional outputs $\Delta\theta_G = \Delta\delta_1$ and $\Delta\omega_G = \Delta\omega_1$ are fictitious, and are used only for the global reference frame transformation, while the measurement output $\Delta\omega^{\rm sg} = \mathrm{col}(\Delta\omega_1, \dots, \Delta\omega_{n_{\rm sg}})$ will be used for control purposes.

D. *Power Converter Model (Grid-Following)*

In this paper, it is sufficient to model inverters using an *average* model thus ignoring discontinuous high-frequency switching dynamics [26]. The dynamic model of the kth power inverter consists of the RL output filter dynamics with output current states $i^{\rm o}_{{\rm dq},k} = \mathrm{col}(i^{\rm o}_{{\rm d},k}, i^{\rm o}_{{\rm q},k})$; a sixth-order phase-locked loop with internal states $x_{{\rm PLL},k} \in \mathbb{R}^5$, and output voltage angle state $\delta_k \in \mathbb{R}$ [27]; and a PI current control loop with $\rm dq$ decoupling cross terms with states $\gamma_{{\rm dq},k} \in \mathbb{R}^2$. The input to the kth inverter model is the terminal voltage $v_{{\rm dq},k} \in \mathbb{R}^2$ with the injected grid current $i_{{\rm dq},k}$ as the output. Omitting a detailed derivation, the final vectorized model of all inverters with inputs and outputs in the global $\rm dq$ frame is given by:

$$\begin{aligned} \dot{x}^{\rm pc} &= f^{\rm pc}(x^{\rm pc}, \theta_G, V^{\rm pc}_{\rm DQ}) \\ I^{\rm pc}_{\rm DQ} &= h^{\rm pc}(x^{\rm pc}, \theta_G) \end{aligned} \tag{16}$$

and around an operating point, one obtains the following associated linearized model:

$$\Delta\dot{x}^{\rm pc} = A^{\rm pc}\Delta x^{\rm pc} + B^{\rm pc}_G\Delta\theta_G + B^{\rm pc}_{\rm DQ}\Delta V^{\rm pc}_{\rm DQ} \tag{17a}$$

$$\Delta I^{\rm pc}_{\rm DQ} = C^{\rm pc}_{\rm DQ}\Delta x^{\rm pc} + D^{\rm pc}_G\Delta\theta_G \,. \tag{17b}$$

E. *Interconnected Microgrid Model*

A general method for interconnecting the preceding component models and the network model are discussed next. First, define the *indicator matrices* $\mathrm{I}_{\rm ld} \in \{0,1\}^{n_{\rm b}\times n_{\rm ld}}$, $\mathrm{I}_{\rm sg} \in \{0,1\}^{n_{\rm b}\times n_{\rm sg}}$, and $\mathrm{I}_{\rm pc} \in \{0,1\}^{n_{\rm b}\times n_{\rm pc}}$. These matrices are defined component-wise as, for example, element (k,g) of $\mathrm{I}_{\rm sg}$ equals 1 if generator $g \in \mathcal{N}_{\rm sg}$ is connected to bus $k \in \mathcal{N}_{\rm b}$, and zero otherwise. To use these matrices in $\rm dq$ coordinates, let $\mathcal{I}_{\rm ld} = \mathrm{I}_{\rm ld} \otimes \mathrm{Id}_2$, $\mathcal{I}_{\rm sg} = \mathrm{I}_{\rm sg} \otimes \mathrm{Id}_2$, and $\mathcal{I}_{\rm pc} = \mathrm{I}_{\rm pc} \otimes \mathrm{Id}_2$. The indicator matrices are used to sum the global $\rm dq$ current injections at each bus, yielding:

$$I^{\rm ext}_{\rm DQ} = \mathcal{I}_{\rm ld}I^{\rm ld}_{\rm DQ} + \mathcal{I}_{\rm sg}I^{\rm sg}_{\rm DQ} + \mathcal{I}_{\rm pc}I^{\rm pc}_{\rm DQ} = \mathcal{I}\begin{bmatrix} I^{\rm ld}_{\rm DQ} \\ I^{\rm sg}_{\rm DQ} \\ I^{\rm pc}_{\rm DQ} \end{bmatrix} \tag{18}$$

where $\mathcal{I} = \left[\mathcal{I}_{\rm ld}\ \mathcal{I}_{\rm sg}\ \mathcal{I}_{\rm pc}\right]$. Similarly, the voltage potential inputs for the subsystem models can be determined as follows:

$$\begin{bmatrix} V^{\rm ld}_{\rm DQ} \\ V^{\rm sg}_{\rm DQ} \\ V^{\rm pc}_{\rm DQ} \end{bmatrix} = \begin{bmatrix} \mathcal{I}^{\mathsf T}_{\rm ld}V_{\rm DQ} \\ \mathcal{I}^{\mathsf T}_{\rm sg}V_{\rm DQ} \\ \mathcal{I}^{\mathsf T}_{\rm pc}V_{\rm DQ} \end{bmatrix} = \mathcal{I}^{\mathsf T}V_{\rm DQ} \,. \tag{19}$$

The overall nonlinear microgrid model is formed by the nonlinear network equations (5), the exponential load equations (10), the synchronous generator model (14), the inverter model (16), and the interconnection equations (18), (19). A block diagram schematic is shown in Figure 1.

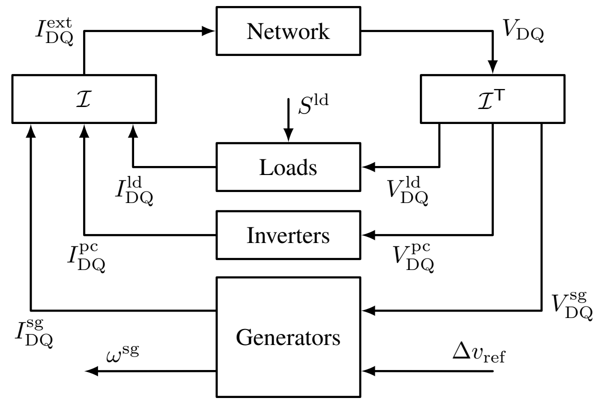

Fig. 1: Block diagram of interconnected microgrid model.

The overall open-loop linearized microgrid model with state $\Delta x^{\rm mg} = \mathrm{col}(\Delta x^{\rm net}, \Delta x^{\rm sg}, \Delta x^{\rm pc})$ is obtained from (6), (11), (15), (17), (18), and (19) as follows:

$$\begin{aligned} \Delta\dot{x}^{\rm mg} &= A^{\rm mg}\Delta x^{\rm mg} + B^{\rm mg}_S\Delta S^{\rm ld} + B^{\rm mg}_v\Delta v_{\rm ref} \\ \Delta\omega^{\rm sg} &= C^{\rm mg}\Delta x^{\rm mg} \end{aligned} \tag{21}$$

where the system matrices are defined in (20).

Remark (Incorporating other components): The modelling framework developed is modular, and can easily incorporate other component models including grid-forming and grid-following power converters, or machine and convertor models of different order. This is easily concluded from Fig. 1, where additional model types simply correspond to new component blocks, with the interconnection matrices $\mathcal{I}$ being expanded accordingly. The only requirement is that the component be described by an admittance-type model, with terminal voltage being the input and terminal current being the output. □

*The selection of a constant global reference frequency $\omega_{\rm G} = \omega_{\rm bse}$ is also common, but is inappropriate for systems without governors; the choice $\omega_{\rm G} = \omega_1$ allows for this possibility at the expense of more complicated formulas.

$$
\begin{aligned}
A^{\mathrm{mg}} = & \underbrace{\left[\begin{array}{c|c|c} A^{\mathrm{net}} & \mathbb{0} & \mathbb{0} \\ \hline \mathbb{0} & A^{\mathrm{sg}} & \mathbb{0} \\ \hline \mathbb{0} & \mathbb{0} & A^{\mathrm{pc}} \end{array}\right]}_{\text{subsystem dynamics}} + \left[\begin{array}{c|c|c} B_{\mathrm{DQ}}^{\mathrm{net}} & \mathbb{0} & \mathbb{0} \\ \hline \mathbb{0} & B_{\mathrm{DQ}}^{\mathrm{sg}} & \mathbb{0} \\ \hline \mathbb{0} & \mathbb{0} & B_{\mathrm{DQ}}^{\mathrm{pc}} \end{array}\right] \underbrace{\left[\begin{array}{c|c|c} \mathcal{I}_{\mathrm{ld}} A^{\mathrm{ld}} \mathcal{I}_{\mathrm{ld}}^{\mathsf{T}} & \mathcal{I}_{\mathrm{sg}} & \mathcal{I}_{\mathrm{pc}} \\ \hline \mathcal{I}_{\mathrm{sg}}^{\mathsf{T}} & \mathbb{0} & \mathbb{0} \\ \mathcal{I}_{\mathrm{pc}}^{\mathsf{T}} & \mathbb{0} & \mathbb{0} \end{array}\right]}_{\text{interconnection matrix}} \left[\begin{array}{c|c|c} C_{\mathrm{DQ}}^{\mathrm{net}} & \mathbb{0} & \mathbb{0} \\ \hline \mathbb{0} & C_{\mathrm{DQ}}^{\mathrm{sg}} & \mathbb{0} \\ \hline \mathbb{0} & \mathbb{0} & C_{\mathrm{DQ}}^{\mathrm{pc}} \end{array}\right] \\
& + \underbrace{\begin{bmatrix} B_{\mathrm{DQ}}^{\mathrm{net}} \mathcal{I}_{\mathrm{pc}} D_G^{\mathrm{pc}} & B_G^{\mathrm{net}} \\ \mathbb{0} & \mathbb{0} \\ B_G^{\mathrm{pc}} & \mathbb{0} \end{bmatrix} \begin{bmatrix} \mathbb{0} & C_{\theta_G}^{\mathrm{sg}} & \mathbb{0} \\ \mathbb{0} & C_{\omega_G}^{\mathrm{sg}} & \mathbb{0} \end{bmatrix}}_{\text{residual dq transform terms}}, \quad B_v^{\mathrm{mg}} = \begin{bmatrix} \mathbb{0} \\ B_v^{\mathrm{sg}} \\ \mathbb{0} \end{bmatrix}, \; B_S^{\mathrm{mg}} = \begin{bmatrix} B_{\mathrm{DQ}}^{\mathrm{net}} \mathcal{I}_{\mathrm{ld}} E^{\mathrm{ld}} \\ \mathbb{0} \\ \mathbb{0} \end{bmatrix}, \; C^{\mathrm{mg}} = \begin{bmatrix} \mathbb{0} & C_{\omega}^{\mathrm{sg}} & \mathbb{0} \end{bmatrix}
\end{aligned} \tag{20}
$$

III. Optimal VFC Design Problem

A. VFC Design

The guiding principle behind VFC is to measure the frequency deviations $\Delta\omega^{\mathrm{sg}}$ and change the set-points of voltage regulators in the system, to compensate for active power mismatches [15]. For example, in an event of under-frequency, the voltage regulator set-points are decreased, causing a decrease in the provided load voltage, and a subsequent decrease in load power consumption. For a coefficient of $m_k = 1.5$ in (8), which has been shown to be a typical load voltage sensitivity for islanded microgrids [15], [17], a 5% drop in the nominal operating voltage yields a 7.6% drop in the demand.

The design of VFC is formulated here as an optimal control problem for a so-called generalized plant, which is the model within the dashed box in Fig. 2. The generalized plant consists

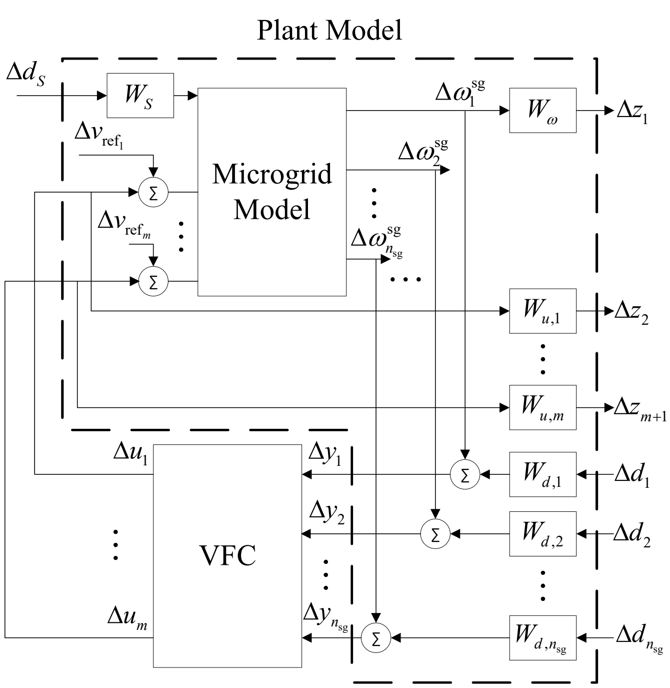

Fig. 2: Systematic VFC Control Synthesis Structure.

of the linearized microgrid model (21) augmented by the following additional equations:

(i) *Control signals*: $\Delta u = \Delta v_{\mathrm{ref}}$ generated by the VFC.

(ii) Frequency *measurement equations*: $\Delta y = \Delta\omega^{\mathrm{sg}} + W_n \Delta d_n$, where $\Delta d_n \in \mathbb{R}^{n_{\mathrm{sg}}}$ models measurement noise and $W_d = \mathrm{diag}(W_{d,1}, \ldots, W_{d,n_{\mathrm{sg}}})$ is a diagonal matrix parameterizing the noise level.

(iii) *load disturbance inputs*: parameterized as $\Delta S^{\mathrm{ld}} = W_S \Delta d_S$, where $d_S \in \mathbb{R}^{2n_{\mathrm{ld}}}$ models the load power disturbances and $W_S = \mathrm{diag}(W_{S,1}, \ldots, W_{S,2n_{\mathrm{ld}}})$ parameterizes the disturbance strengths.

(iv) *system performance outputs*:

$$\Delta z = \mathrm{col}(\Delta z_1, \Delta z_2) = \mathrm{col}(W_\omega \Delta\omega^{\mathrm{sg}}, W_u \Delta u)$$

which contains the set of variables that one wishes the controller to "keep small" in the presence of disturbances, once again weighted using diagonal matrices W_ω and W_u of appropriate sizes.†

In terms of these definitions and the microgrid model (21), the generalized plant $\mathcal{G}$ is given by:

$$
\left[\begin{array}{c} \Delta\dot{x}^{\mathrm{mg}} \\ \hline \Delta z_1 \\ \Delta z_2 \\ \hline \Delta y \end{array}\right] = \left[\begin{array}{c|ccc} A^{\mathrm{mg}} & B_S^{\mathrm{mg}} W_S & \mathbb{0} & B_v^{\mathrm{mg}} \\ \hline W_\omega C^{\mathrm{mg}} & \mathbb{0} & \mathbb{0} & \mathbb{0} \\ \mathbb{0} & \mathbb{0} & \mathbb{0} & W_u \\ \hline C^{\mathrm{mg}} & \mathbb{0} & W_n & \mathbb{0} \end{array}\right] \left[\begin{array}{c} \Delta x^{\mathrm{mg}} \\ \hline \Delta d_S \\ \Delta d_n \\ \hline \Delta u \end{array}\right]
$$

The problem of VFC design may then be posed as follows: design an LTI feedback controller $\mathcal{K}$ with state $\xi(t)$:

$$\mathcal{K}: \quad \begin{aligned} \dot{\xi}(t) &= A_c \xi(t) + B_c \Delta y(t) \\ \Delta u(t) &= C_c \xi(t) + D_c \Delta y(t) \end{aligned} \tag{22}$$

processing noisy frequency measurements Δy and producing voltage regulator set points Δu, such that, when $\mathcal{K}$ is interconnected with the generalized plant $\mathcal{G}$, the influence of disturbances Δd on the performance variable Δz is minimized. The feedback interconnection is denoted by $\mathcal{F}(\mathcal{G}, \mathcal{K})$, which is again an LTI system with input Δd and output Δz, seeking to minimize the $\mathcal{H}_\infty$ norm of $\mathcal{F}(\mathcal{G}, \mathcal{K})$, which is defined as the maximum energy amplification from Δd to Δz as follows:

$$\|\mathcal{F}(\mathcal{G}, \mathcal{K})\|_{\mathcal{H}_\infty} := \sup_{\Delta d \in \mathscr{L}_2, \Delta d \neq 0} \frac{\|\Delta z\|_{\mathscr{L}_2}}{\|\Delta d\|_{\mathscr{L}_2}} \tag{23}$$

where $\|\Delta\eta\|_{\mathscr{L}_2} := \left(\int_0^\infty \|\Delta\eta(t)\|_2^2 \,\mathrm{d}t\right)^{1/2}$ denotes the $\mathscr{L}_2$-norm of the signal $\Delta\eta(t)$ [28]. The (sub)-optimal $\mathcal{H}_\infty$ control problem is then formulated as:

$$\underset{\mathcal{K}}{\text{minimize}} \quad \gamma \qquad \text{subject to} \quad \|\mathcal{F}(\mathcal{G}, \mathcal{K})\|_{\mathcal{H}_\infty} < \gamma \,. \tag{24}$$

†While it is intuitive that the VFC should keep the frequency deviations $\Delta\omega^{\mathrm{sg}}$ small, the control inputs Δu must also be included in the performance output to curb overly aggressive control actions, as in a classical LQR control problem. The weights W_ω and W_u weight the relative sizes of these contributions to the overall size $\|\Delta z\|_2$ of the performance output.

Under standard technical assumptions [28], this minimization problem is well-posed and efficiently solvable via convex optimization.

B. Model Simplification

The optimal control synthesis discussed in Section III yields a VFC with the same number of states as the generalized plant [28]. This can be computationally expensive, and implementing a high-order VFC is difficult in practice, thus it is desirable to reduce the dimensionality of the plant when possible [29]. Luckily, the physical properties typical of most microgrids allow for a natural hierarchical or reduced-order models that approximate well the original model for the purposes of VFC design.

It has been previously speculated that the network in microgrids may not play a significant role in the performance of control and optimization techniques [21], in particular because feeders are short and their capacity is much greater than the maximum system demand [22], [23]. Furthermore, the design of an effective VFC is largely informed by load voltage sensitivity and voltage and frequency control (such as exciter and governor) parameters, and not by network dynamics, topology, or impedance. Hence, it is argued next that the static network model may be completely removed, effectively reducing the microgrid to a single bus.

1) Elimination of Feeders: If the feeders are short and have very low impedance, all points in the network are very close electrically. Practice shows that the voltage drop along a microgrid feeder rarely exceeds 0.02 pu in isolated/islanded microgrids [21]–[23]. Therefor, as the principle of VFC is to adjust voltage levels at loads by modifying the voltage at the point of regulation, the feeders will have negligible impact on VFC performance.

To validate this idea dynamically, based on the microgrid model (21) and computing the Fourier-domain response of the machine frequencies to the voltage regulator setpoints, one has:

$$\begin{aligned}\Delta\omega^{\mathrm{sg}}(\mathbf{j}\omega) &= \left[C^{\mathrm{mg}}(\mathbf{j}\omega I - A^{\mathrm{mg}})^{-1}B_v^{\mathrm{mg}}\right]\Delta v_{\mathrm{ref}}(\mathbf{j}\omega) \\ &= T_\epsilon(\mathbf{j}\omega)\Delta v_{\mathrm{ref}}(\mathbf{j}\omega)\,.\end{aligned} \tag{25}$$

Introducing a parameter $\epsilon \in [0, 1]$, which multiplies the feeder impedances, if $\epsilon = 0$, the feeders are removed, while $\epsilon = 1$ yields the true model. The frequency response of the system with feeders ($\epsilon = 1$) and without feeders ($\epsilon = 0$) is illustrated in Fig. 3, for the parameters of the CIGRE benchmark system [30], which exhibits relatively long (approximately 7 km) feeders. Observe that the response of the system with and without the inclusion of feeders is nearly identical, with only minor deviations occurring at high frequencies. For this figure, the test system has three inputs, which are deviations to the voltage regulators set-points, and one output, which is the system global frequnecy.

2) Balanced Model Truncation: After eliminating the feeders, the the standard model reduction technique of balanced truncation is applied to obtain a reduced-order LTI model which describes the input-output dynamics of the microgrid. The order of the reduced model is chosen to obtain a good match between the frequency responses of the reduced and full-order

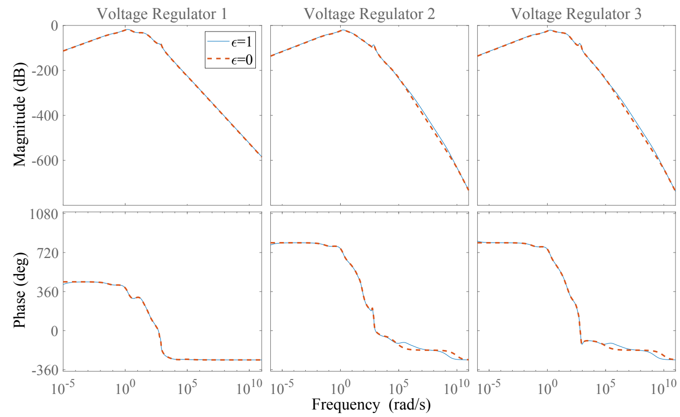

Fig. 3: Frequency response $T_\epsilon(\mathbf{j}\omega)$ for CIGRE system with $\epsilon \in \{0, 1\}$.

models based on [28]. For the test system presented in this paper, the full model order is 117 and is reduced to 10 for controller synthesis.

IV. Simulation Results

This section presents VFC control performance, and evaluates the impact of system simplifications during the design process. A modified version of the CIGRE benchmark for medium voltage distribution network in [30] is used as the test system. This system has three diesel synchronous machine S1, S2, and S3, with a rating of 1.42, 0.86, and 0.57 MVA, respectively. The diesel-based synchronous machines and governors are tuned and validated according the actual measurements from commercial grade synchronous machines in [31], while the exciters are simplified to reduce complexity. In addition, the system has two 1 MW inverters, operating in grid-feeding mode. Loads are modeled using a voltage-sensitive exponential model with a 1.5 exponent, which is a reasonable value for typical isolated microgrids [17].

To illustrate the flexibility one has in terms of VFC control architecture, two VFC designs are considered here. The first design is a standard centralized controller, which processes the frequency measurements from all three synchronous machines, and produces voltage reference changes for the three corresponding exciter systems (a 3×3 controller).

The second design also produces three exciter set-points, but instead processes only the frequency deviation from synchronous machine 1 (a 3×1 controller). For implementation, if the empirical fact that frequency is a global variable in isolated microgrids is exploited (negligible differences throughout the system), one may decentralize this design by letting each unit compute the corresponding regulator setpoint using its *own* frequency deviation instead of that from unit S1:

$$\begin{bmatrix}\mathcal{K}_{11}\\ \mathcal{K}_{21}\\ \mathcal{K}_{31}\end{bmatrix} \approx \begin{bmatrix}\mathcal{K}_{11} & 0 & 0\\ 0 & \mathcal{K}_{21} & 0\\ 0 & 0 & \mathcal{K}_{31}\end{bmatrix}$$

This design is referred to as the decentralized VFC design.

The model simplifications explained in Section. III-B are applied to the system, reducing the overall system states from 117 to 10. The control synthesis is performed using

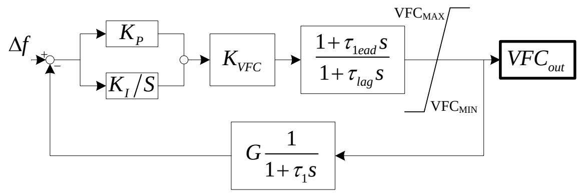

Fig. 4: PI-based VFC based on [15].

TABLE I: Eigenvalues of the system with and without VFC

Without	Centralized	Decentralized	PI-based
-0.0709	-0.0829	-0.0767	-0.0548
-0.1951	-0.0999	-0.1232	-0.1945
-0.8828±1.4117i	-0.1932	-0.1936	-0.2055±0.134i
-1.1465	-0.661±0.152i	-0.508±0.295i	-1.144
-1.1706	-1.1466	1.1424	-1.1689

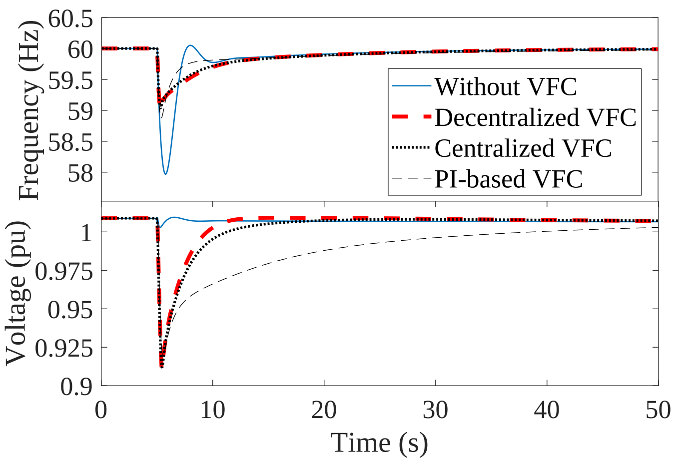

Fig. 5: Frequency and voltage response of the system with and without the VFC.

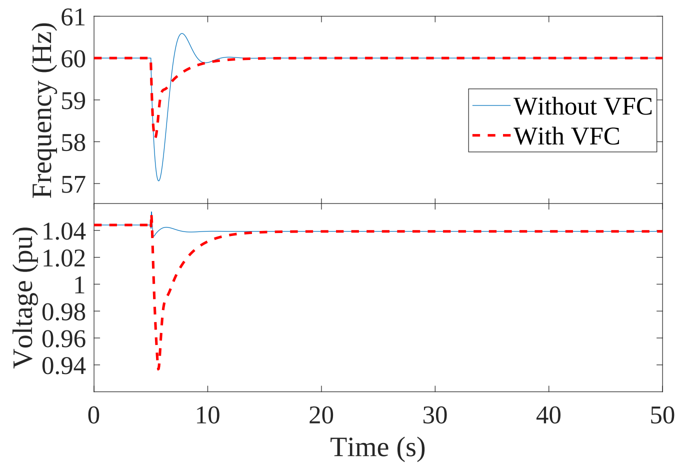

Fig. 6: Frequency and voltage response of the system with and without the VFC with grid supporting converter.

MATLAB bulit-in H infinity synthesis function [32], resulting in a controller with 10 states.

Finally, for the sake of comparison, the performance of a single-input-single-output PI-based VFC design, as shown in Fig. 4, is also included in the result. The feedback loop is added to avoid parallel integration of frequency deviation by the S1 governor and the VFC. This PI-based VFC receives the frequency deviation from S1 and sends the same output signal to all the three exciters, and is tuned by a combination of Ziegler-Nichols and grid-search techniques.

To investigate the impact of VFC, the system loading is suddenly increased by 650 kW, and the system performance with and without VFC is shown in Fig. 5. Prior to the disturbance, the system nominal loading is 2.5 MW of active power and 1 MVar of reactive power. The inverters are injecting a total of 1 MW of active power and 600 kVar of reactive power. S1 is operating in isochronous mode, injecting 625 kW and 480 kVar, while S2 and S3 are operating in constant active power mode, injecting of 548 kW and 440 kW active power correspondingly.

As seen in Fig. 5, the system frequency response is considerably improved, with over 50% decrease in the peak-to-peak value. Moreover, the system damping is also enhanced, as the system with VFC exhibits a critically damped performance. In addition, the steady-state deviation for both voltage and frequency is zero. Although the frequency response with the PI-based VFC has a slightly shorter recovery time, the voltage recovery is considerably slower, demonstrating the major advantage of the design proposed here as compared to a conventional PI-based VFC. Note that the difference between the performance of the two proposed VFC designs is not significant. The results presented here demonstrate the considerable benefit of a well-tuned VFC, acting as a virtual flywheel in the system to compensate for transient active power mismatches in the system.

The impact of the controller on the system eigenvalues is reported in Table. I, which includes the first 5 eigenvalues with the largest real part in order of magnitude. As seen in Table. I, for the centralized and decentralized VFCs, the real part of the system critical eigenvalue is slightly decreased, indicating an improved damping ratio.

To further verify the controller synthesis procedure, S2 and S3 are replaced by a 1 MW grid-supporting inverter. The inverter is set to inject the same active power as S1 and 100 KVar at nominal steady-state terminal voltage. The inverter reactive power injection is sensitive to a terminal voltage set-point through a 1.42 MVar/pu linear droop mechanism. The rest of the system, including the loading and the disturbance is the same as before. Thus, the VFC in this case has one input, S1 frequency, and two outputs that integrate with S1 exciter set-point and the grid-supporting inverter voltage-set point. The system performance is shown in Fig. 6, demonstrating a considerable improvement in the system frequency response. This is continued by the system three eigenvalues with the largest real-part shown in Table II.

V. Conclusions

A scalable and generic model of a hybrid microgrid was first formulated and linearized for general control synthesis purposes. The model was then used to demonstrate the insignificant impact of microgrid feeders on voltage-frequency coupling through mathematical and experimental analysis; the outcome

TABLE II: Eigenvalues of the system with grid-supporting converter with and without VFC

Without VFC	with VFC
-0.8791±1.4824i	-0.6184
-1.2003	-1.2026
-16.0883±13.3779i	-4.5233±4.834

of this analysis laid the foundation for considerable model simplification. An optimal $\mathcal{H}_\infty$ control synthesis framework for VFC was established on the simplified model and tested on the actual model, showing that the synthesis process is robust to model simplifications, and that a well-tuned VFC controller enhances the system damping, as well as its frequency response. Thus, the VFC plays the role of a virtual flywheel with a considerably capacity compared to the system nominal rating. The presented results here illustrate the small role of microgrid feeder on its static and dynamic performance, as well as voltage-frequency coupling. Furthermore, the study presented here lays the foundation on an even more robust VFC designs, considering uncertainty in load and DERs parameters.

REFERENCES

[1] B. Lasseter, "Microgrids [distributed power generation]," in *Proc. of IEEE Power Eng. Soc. Winter Meet.*, Jan. 2001, pp. 146–149.

[2] R. H. Lasseter, J. H. Eto, B. Schenkman, J. Stevens, H. Vollkommer, D. Klapp, E. Linton, H. Hurtado, and J. Roy, "CERTS microgrid laboratory test bed," *IEEE Trans. Power Del.*, vol. 26, pp. 325–332, Jan. 2011.

[3] F. Katiraei, M. Iravani, and P. W. Lehn, "Micro-grid autonomous operation during and subsequent to islanding process," *IEEE Trans. Power Del.*, vol. 20, no. 1, pp. 248–257, Jan. 2005.

[4] D. E. Olivares, A. Mehrizi-Sani, A. H. Etemadi, C. A. Cañizares, R. Iravani, M. Kazerani, A. H. Hajimiragha, O. Gomis-Bellmunt, M. Saeedifard, R. Palma-Behnke, G. A. Jimenez-Estevez, and N. D. Hatziargyriou, "Trends in microgrid control," *IEEE Trans. Smart Grid*, vol. 5, no. 4, pp. 1905–1919, July 2014.

[5] M. Farrokhabadi, C. A. Cañizares, J. W. Simpson-Porco, E. Nasr, L. Fan, P. A. Mendoza Araya, R. Tonkoski, U. Tamrakar, N. Hatziargyriou, D. Lagos, R. W. Wies, M. Paolone, M. Liserre, L. Meegahapola, M. Kabalan, A. H. Hajimiragha, D. Peralta, M. Elizondo, K. P. Schneider, F. Tuffner, J. Reilly, and R. Palma Behnke, "Microgrid stability, definitions, analysis, and modeling," IEEE Power and Energy Society, Tech. Rep., Apr. 2018.

[6] G. Dellile, B. Francois, and G. Malarange, "Dynamic frequency control support by energy storage to reduce the impact of wind and solar generation on isolated power system's inertia," *IEEE Trans. Sustain. Energy*, vol. 3, no. 4, pp. 931–939, Oct. 2012.

[7] A. H. Hajimiragha, M. R. Dadash Zadeh, and S. Moazeni, "Microgrids frequency control considerations within the framework of the optimal generation scheduling problem," *IEEE Trans. Smart Grid*, vol. 6, no. 2, pp. 534–547, Mar. 2015.

[8] J. M. Guerrero, M. Chandorka, T. Lee, and P. C. Loh, "Advanced control architectures for intelligent microgrids–part I: Decentralized and hierarchical control," *IEEE Trans. Ind. Electron.*, vol. 60, no. 4, pp. 1254–1262, April 2012.

[9] J. M. Guerrero, P. C. Loh, T. Lee, and M. Chandorkar, "Advanced control architectures for intelligent microgrids–part II: Power quality, energy storage, and AC/DC microgrids," *IEEE Trans. Ind. Electron.*, vol. 60, no. 4, pp. 1263–1270, April 2012.

[10] R. Majumder, G. Ledwich, A. Ghosh, S. Chakrabarti, and F. Zare, "Droop control of converter-interfaced microsources in rural distributed generation," *IEEE Trans. Power Del.*, vol. 25, no. 4, pp. 2768–2778, March 2010.

[11] Y. A.-R. I. Mohamed and E. F. El-Saadany, "Adaptive decentralized droop controller to preserve power sharing stability of paralleled inverters in distributed generation microgrids," *IEEE Trans. Power Electron.*, vol. 23, no. 6, pp. 2806–2816, Nov. 2008.

[12] Y. Xu, W. Zhang, G. Hug, S. Kar, and Z. Li, "Cooperative control of distributed energy storage systems in a microgrid," *IEEE Trans. Smart Grid*, vol. 6, no. 1, pp. 238–248, Jan. 2015.

[13] A. H. Etemadi, E. J. Davison, and R. Iravani, "A decentralized robust control strategy for multi-der microgridspart I: Fundamental concepts," *IEEE Trans. Power Del.*, vol. 27, no. 4, pp. 1843–1853, Oct. 2012.

[14] Q. Lv, G. Yang, H. Geng, and X. Zhang, "Hybrid cooperative control method for microgrid with large generation or load fluctuations," *The Journal of Engineering*, vol. 2017, no. 13, pp. 1896–1900, Oct. 2017.

[15] M. Farrokhabadi, C. A. Cañizares, and K. Bhattacharya, "Frequency control in isolated/islanded microgrids through voltage regulation," *IEEE Trans. Smart Grid*, vol. 8, no. 3, pp. 1185–1194, Oct. 2015.

[16] M. Farrokhabadi, C. A. Cañizares, and K. Bhattacharya, "A voltage-based frequency controller for inverter-based systems in microgrids," in *Proc. IEEE Power Eng. Soc. Gen. Meeting*, Boston, MA, July 2016, pp. 1–5.

[17] G. Delille, L. Capely, D. Souque, and C. Ferrouillat, "Experimental validation of a novel approach to stabilize power system frequency by taking advantage of load voltage sensitivity," in *Proc. of IEEE PowerTech.*, Eindhoven, Netherlands, June 2015.

[18] M. Diaz-Aguilo, J. Sandraz, R. Macwan, F. de Leon, D. Czarkowski, C. Comack, and D. Wang, "Field-validated load model for the analysis of CVR in distribution secondary networks: Energy conservation," *IEEE Trans. Power Del.*, vol. 28, no. 4, pp. 2428 – 2436, Oct. 2013.

[19] F. Katiraei, M. Iravani, and P. Lehn, "Small-signal dynamic model of a micro-grid including conventional and electronically interfaced distributed resources," *IET Gen. Trans. Dist.*, vol. 1, no. 3, pp. 369 – 378, May 2017.

[20] N. Pogaku, M. Prodanovic, and T. C. Green, "Modeling, analysis and testing of autonomous operation of an inverter-based microgrid," *IEEE Trans. Power Electron.*, vol. 22, no. 2, pp. 613–625, Mar. 2007.

[21] B. V. Solanki, C. A. Canizares, and K. Bhattacharya, "Practical energy management systems for isolated microgrids," *IEEE Trans. Smart Grid*, Early Access.

[22] R. Palma-Behnke, C. Benavides, F. Lanas, B. Severino, L. Reyes, J. Llanos, and D. Saez, "A microgrid energy management system based on the rolling horizon strategy," *IEEE Trans. Smart Grid*, vol. 4, no. 2, pp. 996–1006, June 2013.

[23] A. H. Hajimiragha and M. R. D. Zadeh, "Research and development of a microgrid control and monitoring system for the remote community of Bella Coola: Challenges, solutions, achievements and lessons learned," in *Proc. IEEE Int. Conf. on Smart Energy Grid Eng. (SEGE)*, Oshawa, Canada, Aug. 2001.

[24] F. Dörfler, J. W. Simpson-Porco, and F. Bullo, "Electrical networks and algebraic graph theory: Models, properties, and applications," *Proceedings of the IEEE*, vol. 106, pp. 977–1005, May 2018.

[25] P. W. Sauer and M. A. Pai, *Power System Dynamics and Stability*, 1998.

[26] M. Farrokhabadi, S. König, C. A. Cañizares, K. Bhattacharya, and T. Leibfired, "Battery energy storage system models for microgrid stability analysis and dynamic simulation," *IEEE Trans. Power Syst.*, vol. 33, no. 2, pp. 2301–2312, Mar. 2018.

[27] A. Yazdani and R. Iravani, *Voltage-Sourced Converters in Power Systems: Modeling, Control, and Applications*. Hoboken, New Jersey: Wiley-IEEE Press, 2010.

[28] G. E. Dullerud and F. Paganini, *A Course in Robust Control Theory*, ser. Texts in Applied Mathematics. Springer-Verlag, 2000, no. 36.

[29] D. Henrion, "H-infinity controller design on the compleib problems with the robust control toolbox for matlab," LAAS-CNRS Research Report, Tech. Rep., Oct. 2005.

[30] K. Strunz, E. Abbasi, C. Abbey, C. Andrieu, U. Annakkage, S. Barsali, R. C. Campbell, R. Fletcher, F. Gao, T. Gaunt, A. Gole, N. Hatziargyriou, R. Iravani, G. Joos, H. Konishi, M. Kuschke, E. Lakervi, C. Liu, J. Mahseredjian, F. Mosallat, D. Muthumuni, A. Orths, S. Papathanassiou, K. Rudion, Z. Styczynski, and S. C. Verma, "Benchmark systems for network integration of renewable and distributed energy resources," Cigre Task Force C6.04.02, Tech. Rep., May 2013.

[31] M. Arriaga and C. A. Cañizares, "Overview and analysis of data for microgrid at kasabonika lake first nation (KLFN)," Hatch Project Confidential Report, University of Waterloo, Tech. Rep., Sep. 2015.

[32] "h2hinfsyn." [Online]. Available: https://www.mathworks.com/help/robust/ref/h2hinfsyn.html